Evaluation of Magnetic Materials for Very High Frequency Power Applications

Evaluation of Magnetic Materials for Very High Frequency Power Applications

Yehui Han, *Member, IEEE,* Grace Cheung, An Li, Charles R. Sullivan, *Member, IEEE,* and David J. Perreault, *Senior Member, IEEE*

***Abstract*—This paper investigates the loss characteristics of rf magnetic materials for power conversion applications in the 10 MHz to 100 MHz range. A measurement method is proposed that provides a direct measurement of inductor quality factor Q_L as a function of inductor current at rf frequencies, and enables indirect calculation of core loss as a function of flux density. Possible sources of error in measurement and calculation are evaluated and addressed. The proposed method is used to identify loss characteristics of several commercial rf magnetic core materials. The loss characteristics of these materials, which have not previously been available, are illustrated and compared in tables and figures. The use of the method and data are demonstrated in the design of a magnetic-core inductor, which is applied in a 30 MHz inverter. The results of this paper are thus useful for design of magnetic components for very high frequency (VHF) applications.**

***Index Terms*—Magnetic materials, resonant inductor, very high frequency (VHF), Steinmetz parameters.**

I. Introduction

There is a growing interest in switched-mode power electronics capable of efficient operation at very high switching frequencies (e.g., 10 – 100 MHz). Power electronics operating at such frequencies include resonant inverters [1]–[10] (e.g., for heating, plasma generation, imaging, and communications) and resonant dc-dc converters [1], [3], [11]–[20] (which utilize high frequency operation to achieve small size and fast transient response.) These designs utilize magnetic components operating at high flux levels, and often under large flux swings. Moreover, it would be desirable to have improved magnetic components for rf circuits such as matching networks [21]–[25]. There is thus a need for magnetic materials and components suitable for operation under high flux swings at frequencies above 10 MHz.

Unfortunately, most magnetic materials exhibit unacceptably high losses at frequencies above a few megahertz. Moreover, the few available bulk magnetic materials, which are potentially suitable for frequencies above 10 MHz, are typically only characterized for small-signal drive conditions, and not under the high flux-density conditions desired for power electronics. These characterizations are necessary for effective design of very high frequency power magnetic components [26]. This motivates better characterization of magnetic materials for high-frequency power conversion applications.

This paper, which expands upon an earlier conference paper [27], investigates the loss characteristics of several commercial rf magnetic materials under large-signal ac flux conditions for frequencies above 10 MHz. A measurement method is proposed that provides a direct, accurate measurement of inductor quality factor Q_L as a function of ac current amplitude at rf frequencies. This method also yields an accurate measurement of loss density of a core material as a function of flux density at rf frequencies. We use this technique to identify the loss characteristics of several different rf magnetic materials at frequencies up to 70 MHz.

Section II of the paper introduces a method for accurately measuring the quality factor of rf inductors under large signal drive conditions. Section III shows how to utilize these measurements to identify core loss characteristics as a function of flux density and frequency. In Section IV, we employ these techniques to identify the loss characteristics of several commercial rf magnetic-core materials. These loss characteristics, which have not previously been available except to the authors, are presented and compared in tables and figures. Section V illustrates the application of this data in the design of a resonant inductor, which is applied in a 30 MHz resonant inverter. Finally, Section VI concludes the paper.

II. Measuring the Quality Factor of RF Inductors

A. Measurement Circuit and Principles

The quality factor Q_L of a magnetic-core inductor is a function of both operating frequency and ac current (or flux) level. We utilize a measurement circuit that enables Q_L to be determined at a single specified frequency across a wide range of drive levels. Inductor quality factor is simply determined as the ratio of amplitudes of two ground-referenced voltages in a resonant circuit. A schematic of the measurement circuit is shown in Fig. 1. L, R_{cu} and R_{core} model the inductor to be evaluated: L is its inductance, R_{cu} represents its copper loss and R_{core} represents its core loss at a single frequency. R_C and C model a resonant capacitor selected to resonate with the inductor at the desired frequency. C is its capacitance and R_C represents its equivalent series resistance. The input voltage V_{in} should ideally be a pure sinusoidal wave, and is generated by a signal generator and a rf power amplifier. The amplitude and frequency of V_{in} can be tuned by the signal generator.

Y. Han is with the University of Wisconsin-Madison, 2559C Engineering Hall, 1415 Engineering Drive, Madison, WI 53706 USA (e-mail: yehui@engr.wisc.edu).

G. Cheung is with Intersil Corp (e-mail: gmcheung@gmail.com).

A. Li is with Massachusetts Institute of Technology, MA 02139 USA (e-mail: anli@mit.edu).

C. R. Sullivan is with Thayer School of Engineering at Dartmouth, Hanover, NH 03755 USA (e-mail: charles.r.sullivan@dartmouth.edu).

D. J. Perreault is with Laboratory for Electromagnetic and Electronic Systems, Massachusetts Institute of Technology, Cambridge, MA 02139 USA (e-mail: djperrea@mit.edu).

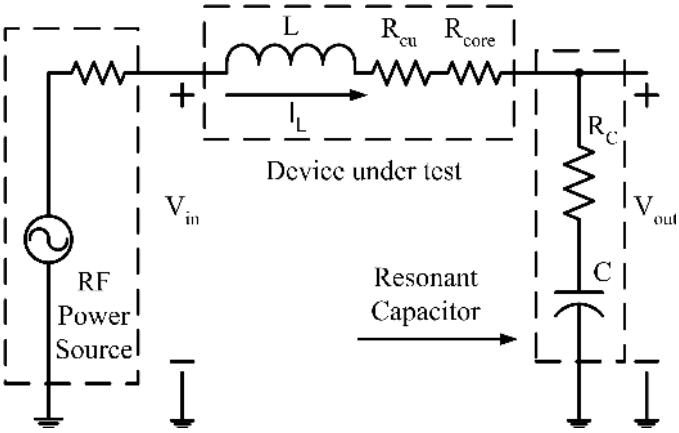

Fig. 1. Schematic of the circuit for measuring inductor quality factor, which can be calculated as the amplitude ratio V_{out-pk} over V_{in-pk}. (The resonant capacitor's ESL is neglected.)

To understand how this circuit enables direct measurement of inductor Q_L , consider that at the resonant frequency:

$$f_s = \frac{\omega_s}{2\pi} = \frac{1}{2\pi\sqrt{LC}} \tag{1}$$

The ratio between the output voltage amplitude V_{out-pk} and the input voltage amplitude V_{in-pk} is:

$$\begin{aligned}\frac{V_{out-pk}}{V_{in-pk}} &= \left|\frac{V_{out}(j\omega_s)}{V_{in}(j\omega_s)}\right| = \left|\frac{R_C + \frac{1}{j\omega_s C}}{R_{core}+R_{cu}+R_C}\right| \\ &\approx \frac{\omega_s L}{R_{core}+R_{cu}} = Q_L \end{aligned} \tag{2}$$

To better illustrate the measurement principles, R_C is ignored in (2) at first and is included in (13) later. The final approximation in (2) is accurate for the case in which R_C is small compared to $R_{cu}+R_{core}$ and to $\frac{1}{j\omega_s C}$, and becomes precisely true when $R_C = 0$. The above equation shows that the ratio of V_{out-pk} and V_{in-pk} is approximately equal to the quality factor of the inductor at the resonant frequency. Probing the two voltages enables direct determination of inductor Q_L. Drive level can be adjusted by varying the amplitude of the rf source. The current of the inductor is equal to the capacitor current and can be calculated from the output voltage and the known capacitor impedance. (These considerations motivate the use of high-precision low loss capacitors such as mica or porcelain capacitors. In our experiments, we have employed microwave porcelain multilayer capacitors from American Technical Ceramics. The equivalent series inductance (ESL) of these capacitors is very small such that it can be ignored in our measurements without introducing significant error.)

One subtlety with this measurement method is the challenge of knowing the precise resonant frequency (for which (1) and (2) apply). Given the small values of inductance that are typically of interest in the $10-100$ MHz range (e.g., inductances of tens to hundreds of nanoHenries [1], [2], [13]), and the correspondingly small values of resonant capacitances (tens to hundreds of picoFarads), parasitic capacitances of the measurement circuit and voltage probes can have a significant impact on the resonant frequency. Considering these influences, the resonant frequency may have up to a 5% deviation from its calculated theoretical value (for typical component values, consistent with experimental observation).

To address this issue, we pre-calculate the capacitor value to achieve the approximate resonant frequency, then adjust the frequency around the calculated resonant frequency to find the frequency point f_s' where $\frac{V_{out-pk}}{V_{in-pk}}$ has the maximum value. Let $R_L = R_{cu} + R_{core}$ represent the total source of loss in the inductor. R_C is ignored in (3), (4) and (5) as it is usually much smaller than R_L. From (2), the derivative of $\frac{V_{out-pk}}{V_{in-pk}}$ with respect to frequency is:

$$\frac{d}{d\omega}\left(\frac{V_{out-pk}}{V_{in-pk}}\right) = -\omega C \frac{CR_L^2 + 2L(\omega^2 LC - 1)}{[\omega^2 C^2 R_L^2 + (\omega^2 LC-1)^2]^{1.5}} \tag{3}$$

Setting $\frac{d}{d\omega}\left(\frac{V_{out-pk}}{V_{in-pk}}\right) = 0$, we find that $\frac{V_{out-pk}}{V_{in-pk}}$ reaches its maximum value at a frequency:

$$f_s' = \frac{\omega_s'}{2\pi} = \frac{1}{2\pi}\sqrt{\frac{1}{LC} - \frac{R_L^2}{2L^2}} \tag{4}$$

From (1) and (2),

$$f_s' = f_s\sqrt{1 - \frac{1}{2Q_L^2}} \tag{5}$$

As $Q_L \gg 1$ for all cases of interest, this actual operating frequency f_s' is approximately equal to the resonant frequency f_s. (The effect of the difference in frequency will be addressed in Section III-C)

B. Measurement Procedures

Before beginning the measurements, an inductor is fabricated based on the frequencies and the range of flux density amplitude B_{pk} of interest. The impedance analyzer we use to measure inductance, capacitance, R_{cu} and R_C is an Agilent 4395A. Prior to using it, the machine is calibrated, and devices with known characteristics are tested to validate the calibration of the machine. We have found that this machine can measure an impedance larger than 10 mΩ with good accuracy in the frequency range of 10 MHz to 100 MHz). The step-by-step measurement procedures are as follows:

1) Measure the inductance: At the resonant frequency f_s, both the inductance L and the quality factor Q_L of the fabricated inductor are measured (under small-signal conditions) using the impedance analyzer. From the measured L, the resonant capacitor value can be calculated. From the measured small-signal Q_L, the expected quality factor under high-power conditions (which should be smaller than the measured small signal Q_L) can be estimated. Though the measurement is under very low drive conditions, the core loss can't be ignored for some materials, so this small-signal Q_L measurement may reflect both core and copper loss.

2) Calculate the relative permeability μ_r: Though most core companies will specify the relative permeability μ_r of the material, μ_r should be measured and calculated to get an accurate value. Assuming that the inductor core is toroidal, from [28] we get:

$$\mu_r \approx \frac{2\pi L}{N^2 h \mu_0 \ln\left(\frac{d_o}{d_i}\right)} \tag{6}$$

where L is the inductance measured in step 1), h, d_o and d_i are the height, the outer diameter and the inner diameter of the inductor, and N is the number of turns of the inductor [1]. To minimize the error caused by the inductance of a single turn loop [28] and leakage flux, N should be as large as possible in a single layer. (In our experiments, we often fabricate and measure another inductor with the same core but a high turns number (> 20) specifically to reduce the single turn inductance error and get an accurate value of μ_r.)

3) Select resonant capacitor: The resonant capacitor value C can be calculated from (1). C should be much larger than the potential parasitic capacitance and the probe capacitance. The precise value C and ESR R_C of the capacitor is also measured using the impedance analyzer. Q_C can be calculated from C and R_C. We assume Q_C is constant during all the measurements. When Q_C is 1000 or higher, it may be difficult to accurately measure its value. In this case, Q_C may be estimated based on data sheet values. Q_C should be ten times larger than Q_L to minimize its influence on the Q_L measurement and the loss extraction (as may be expected from straightforward calculation).

4) Fabricate the resonant circuit: The printed circuit board should be designed carefully to minimize parasitic inductance and capacitance.

5) Calculate the required V_{out}: The inductor current amplitude I_{L-pk} can be calculated from B_{pk} and the inductors parameters. For example, the I_{L-pk} of a toroidal inductor can be calculated as:

$$I_{L-pk} = \frac{\pi(d_o + d_i)B_{pk}}{2\mu_r\mu_0 N} \tag{7}$$

where B_{pk} is the flux density amplitude in the toroidal core. I_{L-pk} is also the current amplitude of the resonant capacitor. The output voltage amplitude V_{out-pk} can be calculated from I_{L-pk} and the impedance of the resonant capacitor:

$$V_{out-pk} = \frac{I_{L-pk}}{2\pi f_s C} = \frac{(d_o + d_i)B_{pk}}{4 f_s C \mu_r \mu_0 N} \tag{8}$$

Using (7) and (8) to calculate I_{L-pk} and V_{out-pk} might not be accurate if μ_r varies significantly with flux density. In such cases, given that there are probes on voltage on both sides of the inductor, inductor voltage could be calculated and integrated to get flux linkage and thus a flux density measurement independent of permeability. In our measurements, we found μ_r to be almost constant across drive level because the actual operating frequency f_s' changed very little ($< 1\%$ by experimental observation) with flux density variation (see Step 7). So the variation of permeability with flux density was not an issue in our data set.

6) Set up the experiment: The experimental setup comprises a signal generator, an rf power amplifier, and an oscilloscope in addition to the fabricated resonant circuit. The signal generator drives the power amplifier to produce a sinusoidal voltage with a variable amplitude and a tunable frequency. In our system we employ an Agilent 33250A signal generator and an AR 150A100B rf power amplifier. The output of the amplifier is connected to the input of the resonant circuit by a matched cable, with any impedance transformation and/or filtering applied at the resonant circuit input. In our system, we typically employ an AVTECH AVX-M4 transmission line transformer ($50:3$ impedance transformation ratio) to better match the $50\ \Omega$ power amplifier to the low-impedance resonant circuit.

Note that the capacitance of the probe that measures the output voltage should be as small as possible, as it adds to the resonant capacitor value. The probe capacitance can be estimated from the data sheet. Here we include it with other parasitic capacitances and have considered its influence in our measurements. The capacitance of the probe to measure the input voltage doesn't influence the measurement results.

7) Measure a set of V_{in-pk} and V_{out-pk}: The signal frequency is initially set to the calculated value of the resonant frequency f_s. However, due to parasitics, probe capacitance and component errors, this frequency is not exactly equal to the resonant frequency f_s. While adjusting the circuit input voltage amplitude manually to maintain the designed V_{out-pk} according to (8), tune the input signal frequency finely and also manually and search for the minimum V_{in-pk}. (The scope we used is a Tektronix TDS520B which has vertical accuracy to 1% and 500 MHz bandwidth. The probes we used in measurements are PMK PHV 621 with a high accuracy and a bandwidth up to 400 MHZ. It may be expected that the ratiometric accuracy of the voltage measurements is still much higher.) The frequency where V_{in} reaches its minimum is f_s' which is close to f_s when Q_L is high.

Because the resonant circuit is highly tuned, the output voltage will be a very good sinusoidal waveform. However, because both the input power and input voltage V_{in} are small, the power amplifier may work in a nonlinear region and a distorted V_{in} may be observed. In this case, a transformer or a low-pass filter at the resonant circuit input can help to reduce the distortion. If the distortion can't be ignored, the amplitude of V_{in} at f_s' can be calculated numerically by Fourier analysis. Using the tuning characteristics, we can also determine if μ_r varies significantly with current level. If μ_r changes, the inductance will change and the tuned resonant frequency f_s' will also change. If this happens, the inductance L and the relative permeability μ_r need to be recalculated based on the resonant capacitor value C and the tuned f_s' . Knowing V_{in-pk} and V_{out-pk}, Q_L can be calculated from (2).

As the quality factor Q_L is usually high in our measurements, the power loss of the inductor is small and the heat is dissipated very well. We also employed computer fans for cooling off the inductor. So the inductor temperature is kept reasonably to the ambient.

Fig. 2 shows a representative curve of Q_L vs. current drive level at 30 MHz for a 190 nH inductor wound with 5 turns of foil (0.116 in wide, 4 mil thick) on an M3 ferrite core. R_{cu} in (2) is almost constant in measurements but R_{core} increases with ac current level. R_{core} dominates the total inductors resistance at large current conditions. So the strong variation of Q_L with ac current level (owing to core loss) is readily

[1]The relative permeability can be also addressed in a complex form which is equal to $\mu_r' - \mu_r'' j$. μ_r' is equal to μ_r in (6) and μ_r'' represents the loss which is also a function of flux density. μ_r'' can be calculated from the core loss measurement results in Section IV. In this paper, we use curves and Steinmetz parameters to represent losses instead of complex permeability.

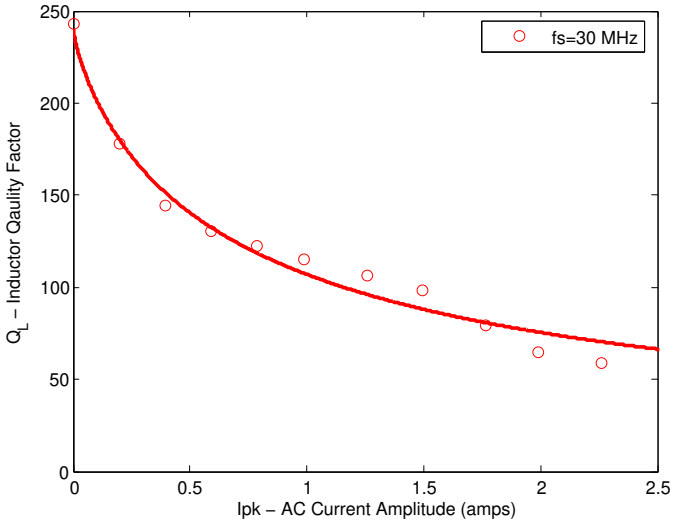

Fig. 2. The Q_L of an inductor fabricated with an M3 toroidal core (OD = 12.7 mm, ID = 7.82 mm, Ht = 6.35 mm) with $N = 5$ turns of 116 mil wide and 4 mil thick foil, and $L = 190$ nH.

observed.

Thermal measurements on the inductors could also be adopted to estimate the losses. However, calorimetric methods are notoriously difficult to use effectively and to calibrate themselves. Consequently, this approach has not been utilized here.

III. EXTRACTION OF LOSS CHARACTERISTICS OF COMMERCIAL RF MAGNETIC CORES

In this section we show how the quality factor measurements of Section II can be adapted to identify core loss characteristics of magnetic materials. We do not seek to identify or model the underlying cause of core losses [29], [30]. Rather, we focus on quantitatively identifying the power loss density of a given magnetic material as a function of flux density under sinusoidal excitation at a specified frequency. Numerous works illustrate how this information can be used in the design of magnetic components, even for systems with complex excitations [31]–[33].

The methods and guidelines exist for direct measurement of core loss through voltage and current measurements made on multi-winding structures [34]–[37]. However, these methods rely on very accurate measurement of phase relationships between voltages and currents, which becomes increasingly hard to do as frequency increases. The method introduced in [37] improves on conventional methods but it still depends on phase shift and has errors due to parasitics of the transformer. Instead, we exploit an indirect method: Starting with an accurate measurement of total inductor loss (from accurate measurement of inductor Q_L), we seek to extract the portion of loss owing to the magnetic core. In the subsections that follow, we describe preparations and measurements of single-layer, foil-wound toroids (of materials to be tested), from which core loss information can be extracted.

A. Design and Fabrication of Low-loss Inductors with Toroidal Cores

To identify the loss characteristics of a magnetic-core material, the quality factors of inductors fabricated with appropriate magnetic cores are measured under large-signal drive conditions. We focus on ungapped toroidal magnetic cores due to the availability of these cores, the simplicity and uniformity of the calculations, and the magnetic self-shielding provided by this core type. Also, the core loss to winding loss ratio is higher in this core type than in other available geometries.

The fabricated inductor should have as small a copper loss as possible compared to its core loss in order to minimize error. For this reason, we utilize a single-layer copper foil winding on the toroidal core. (Even more sophisticated construction techniques are possible [28], but are not used here.)

The copper foil is cut in the shape of a narrow strip. The following equations show the parameters of the copper strip and fabricated inductor.

$$N \approx \sqrt{\frac{2\pi L}{h\mu_r\mu_0 \ln\left(\frac{d_o}{d_i}\right)}} \tag{9}$$

where N is the number of turns, L is the inductance, μ_r is the relative permeability of the magnetic material, μ_0 is the permeability of free space, and h , d_i and d_o are the height, inner diameter and outer diameter of the toroidal core. Note that the thickness t_{cu} of the foil should be much larger than a skin depth in order to get the minimum resistance:

$$t_{cu} \gg \delta = \sqrt{\frac{\rho_{cu}}{\pi\mu_0 f_s}} \tag{10}$$

where ρ_{cu} is the electrical conductivity of copper. For our inductor design, there is little proximity effect and little dc loss, so we don't optimize the foil thickness to minimize the winding loss as in [38]. As long as (10) is satisfied, the copper loss in terms of the thickness is minimized. As shown in (20), the ac copper resistance is decided by the skin depth δ, which is frequency dependent.

The width of the copper foil is selected as:

$$w_{cu} \approx \frac{\pi d_i}{N} \tag{11}$$

to achieve the desired number of turns. In fabrication, a value of w_{cu} is a little smaller than the above value is employed to leave a space between the turns of the foil winding.

The foil winding length is approximately:

$$l_{cu} = N(2h + d_o - d_i) \tag{12}$$

where the length l_{cu} of foil does not include the length of extra copper terminals to be soldered on the PCB pad. Because the relative permeability μ_r of the magnetic core is high ($>$ 4) and the toroidal inductor is self-shielded, we assume that most of the flux is inside the core. Fig. 3 shows an inductor fabricated by the above method. The core is M3-998 from National Magnetics Group.

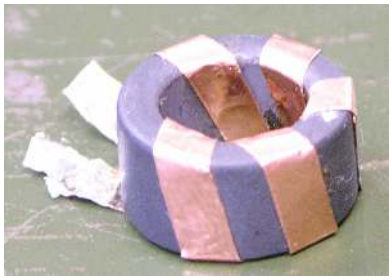

Fig. 3. An example of an inductor fabricated from copper foil and a commercial magnetic core.

B. The Extraction of Core Loss Characteristics from the Measurement Results

The core loss characteristics can be extracted from the measured value of Q_L (based on V_{in-pk}, V_{out-pk} and f_s'). The measured quality factor Q_L provides a measure of the total loss. By subtracting out an estimate of the copper loss, we are left with an estimate of the core loss (and core loss density).

Referring to Fig. 1, we have:

$$Q_L \approx \frac{V_{out-pk}}{V_{in-pk}} = \frac{2\pi f_s L}{R_{core} + R_{cu} + R_C} \tag{13}$$

and

$$R_{core} = \frac{2\pi f_s L V_{in-pk}}{V_{out-pk}} - R_C - R_{cu} \tag{14}$$

The resistance of the resonant capacitor R_C can be measured by the impedance analyzer or acquired through the data sheet. It is more difficult to establish the exact value of R_{cu}. We employ the following method estimate the value for R_{cu}. We fabricate a coreless inductor with the same dimension and measure its R_{cu} using the impedance analyzer. From finite element simulation results, this value is close to the R_{cu} of a magnetic-core inductor for $\mu_r < 4$. When $\mu_r \geq 4$, the value of R_{cu} for a coreless inductor can be lower than the R_{cu} of a magnetic-core inductor by up to 30%. So we consider that this estimation of R_{cu} has up to 30% error. In our experiments, the core loss is controlled to be at least 5 times larger than the copper loss to reduce the error caused by R_{cu}.

With a value for R_{core}, the average core loss can be calculated. We express our results as core loss per unit volume as a function of flux density.

$$P_V = \frac{I_{L-pk}^2 R_{core}}{2V_L} \tag{15}$$

where V_L is the volume of the core. Because B_{pk} is specified, one data point of P_V (mW/cm^3) versus B_{pk} (Gauss) is acquired.

C. The Estimation of Errors

Possible errors in this procedure are discussed below:

1) Error caused by the capacitor ESR: As indicated in (2), capacitor ESR influences the voltage ratio, making it deviate from the desired Q_L value. Capacitor ESR R_C can be measured by the impedance analyzer. When R_C is too small to be measured accurately (e.g., $Q_L > 1000$), the error due to R_C can be estimated. For example, if $Q_L = 100$ and $Q_C > 1000$ by measurement, we estimate Q_C as about 2000 and the error in Q_L caused by R_C will be approximately 5%.

2) Error caused by circuit parasitics: The parasitic parallel capacitance presented by the inductor is typically a few pF. Because the input voltage V_{in} is at least ten times smaller than the output voltage V_{out}, this capacitance can be considered being connected to the ground and combined with other parasitics in parallel with the resonant capacitor. So the circuit schematic in Fig. 1 is still correct. Due to its small value, it has little influence on the resonant circuit. As described preciously, the values of the resonant capacitor and the inductor are controlled to be much larger than the circuit parasitic capacitance or inductance to minimize their influence on the resonant frequency f_s. However, the parasitics can have a very poor Q, (i.e., relatively a high series ac resistance and low parallel ac resistance) which add extra losses. The error can be further reduced by a careful layout. The pads of the resonant inductor should be as close as possible to the pads of the resonant capacitor and the measurement points to reduce the trace inductance and resistance. The resonant capacitor should be also connected to the ground tightly to reduce parasitic series resistance and inductance. With sufficient effort, error due to these parasitics can be made negligibly small and is not considered further in this paper.

3) The error caused by copper loss: The error caused by the copper loss (represented by resistance R_{cu}) can be a severe problem if $R_{core} \leq R_{cu}$. An exact value for the winding resistance R_{cu} is hard to determine. However, if $R_{core} \gg R_{cu}$, the error introduced by inaccuracies in the estimated value of R_{cu} is small. For example, if $R_{core} \geq 5R_{cu}$ and an error of up to 30% in the estimate of R_{cu} occurs, the R_{core} error caused by R_{cu} will be less than 5%. As the core loss increases much faster than the copper loss when the inductor current increases, we select the operating current range to make sure the core loss is at least five times larger than the copper loss.

4) Error caused by the actual operating frequency f_s': Though the difference between f_s' and f_s is small when Q_L is high, the error should be analyzed carefully. Assume the error between the resonant frequency f_s and actual operating frequency f_s' is 1%. While V_{out-pk} is constant, the error of the inductors current is about 1% and the error of the flux density in the inductor core is 1%. If $P_V \propto f_s^{\xi} B_{pk}^{\beta}$, and both ξ and β are about 2.6 to 2.8, the error of P_V will be less than 5.6%. However, the error can be compensated for by knowing f_s' and the approximate value of Q_L.

5) Error caused by uneven flux density: The flux density in a toroidal core is not even, which means the inner part of the core has more power loss than the outer part. This error depends on the dimensions of the core, mainly determined by the ratio of d_o and d_i. For $d_o = 2d_i$ and $\beta = 2.8$, the error is about 10%. However, the error can be also compensated (see [34], for example). As these low permeability magnetic

TABLE I
MATERIALS, SUPPLIERS AND SPECIFICATIONS

Material	Type	Supplier	Permeability
M3	NiZn	National Magnetics Group	12
P	CoNiZn	Ferronics	40
67	NiZn	Fair-rite	40
N40	NiZn	Ceramic Magnetics	15
-17	Powered Iron	Micrometals	4

materials have very high resistivity (e.g., $\approx 10^7$ Ωcm for M3 material), the eddy current in a core is very small and its effect is not considered in this paper.

6) The total error: Considering all these error factors, the total error will be less than 20% (as per the above calculations) if the inductor and the circuit are well designed and fabricated, $R_{core} \gg R_{cu}$, and the measurement is done carefully. All the inductors in our experiments are customized and the dimensions of winding and core are measured accurately, so the construction tolerances are not considered in this paper.

IV. CORE LOSS MEASUREMENTS IN COMMERCIAL MAGNETIC MATERIALS

Here we apply the proposed methods to identify the large signal loss characteristics of several commercial rf magnetic materials. The loss characteristics of these materials under large flux-swing conditions have not been previously available, and are expected to be useful for design of rf power magnetic components. Table I shows the magnetic materials for which data are provided. The loss characteristics of the materials listed in Table I are plotted in Figs. 4 to 8. At 20 MHz, the core loss of -17 material is too small to be measured and extracted. Moreover, it has a useful range extending to higher frequencies. Thus we measured it in a somewhat different range. In Figs. 4 to 8, the Steinmetz equation $P_V = KB_{pk}^{\beta}$ for B_{pk} in Gauss and P_V in mW/cm^3 is used to fit the data. The Steinmetz equation is an empirical means to estimate loss characteristics of magnetic materials [38], [39]. It has many extensions [31]–[33], [38], [40]–[44], but we only consider the formulation for sinusoidal drive at a single frequency here. This consideration can simplify the calculation for data fitting. Table II shows K and β for each of these materials. Note that very high frequency operation (e.g., beyond 20 MHz) can greatly reduce the energy storage requirement for magnetic components as compared to conventional power magnetic frequencies of a few MHz and below, so major size reductions of the power magnetic components can be achieved even at flux density levels of tens to hundreds of Gauss. Owing to core loss considerations, tens to hundreds of Gauss already represent large flux swings at these frequencies, and we consider this as a reasonable operating range for these low-permeability magnetic materials.

We also apply the proposed methods to identify the large signal loss characteristics of 3F3 material from Ferroxcube. 3F3 is a low-frequency high-permeability material often used for power magnetics, and its loss characteristics are known from [45], [46]. In Fig. 9, we compare our measurement results with the manufacturer's data and find they two agree well (errors are within 20% if we assume the manufacturer's

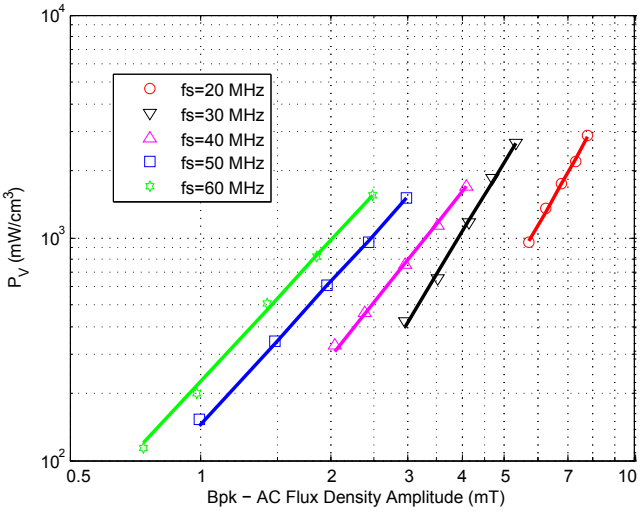

Fig. 4. M3 Material Core Loss vs AC Flux Density.

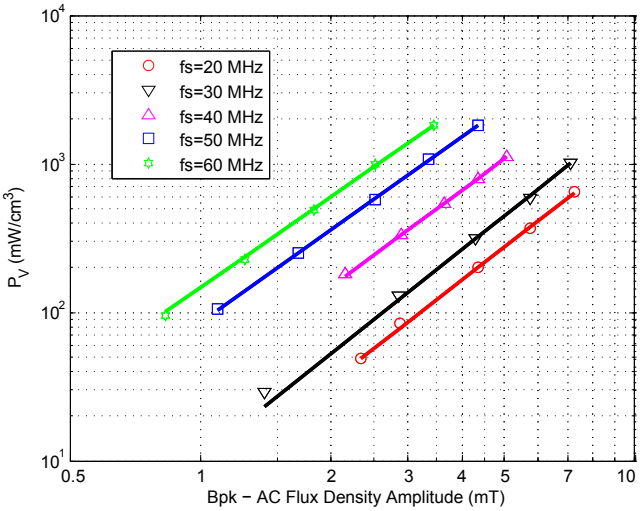

Fig. 5. P Material Core Loss vs AC Flux Density.

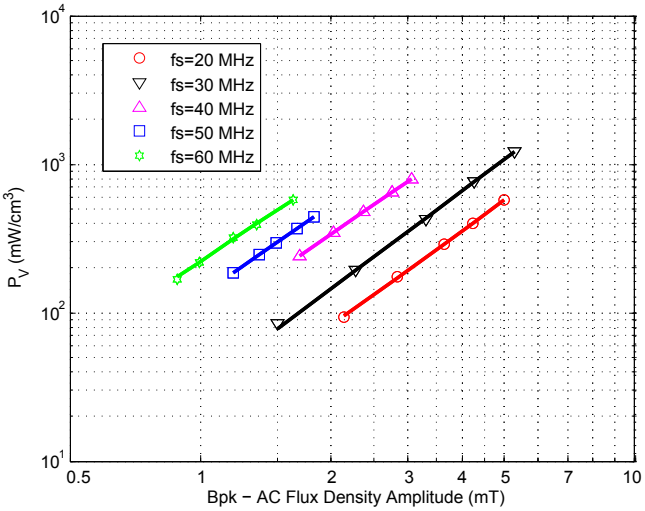

Fig. 6. 67 Material Core Loss vs AC Flux Density.

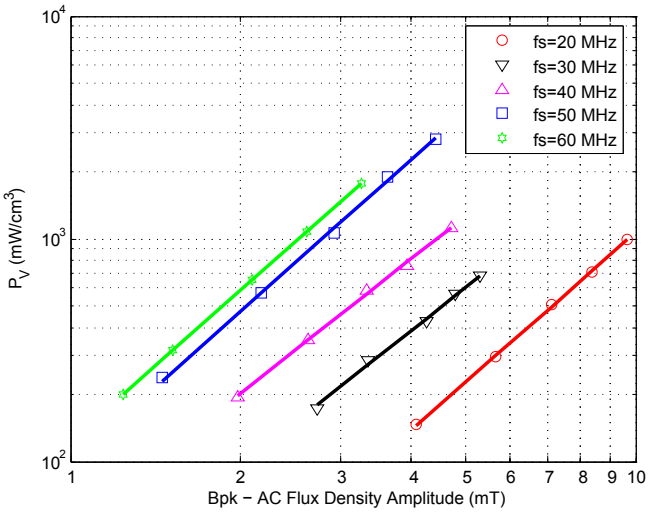

Fig. 7. N40 Material Core Loss vs AC Flux Density.

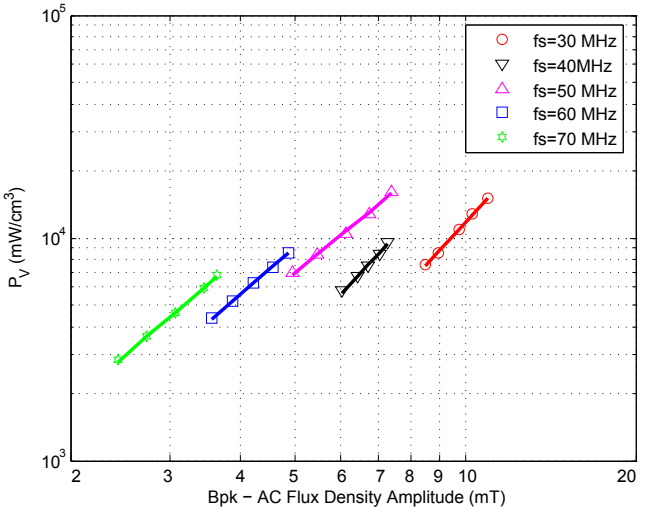

Fig. 8. -17 Material Core Loss vs AC Flux Density. Note that because the permeability of this material is low ($\mu_r = 4$), it is difficult to separate core loss from copper loss. Consequently, the core was operated at extremely high loss densities under forced convection cooling in order to facilitate separation of core loss from copper loss. In many practical designs, one might choose to operate at lower loss densities than utilized here.

TABLE II
STEINMETZ PARAMETERS FOR MATERIALS

	20 MHz		30 MHz	
Material	K	β	K	β
M3	8.28×10^{-4}	3.46	6.75×10^{-3}	3.24
P	3.57×10^{-2}	2.29	5.06×10^{-2}	2.33
67	1.42×10^{-1}	2.12	2.10×10^{-1}	2.18
N40	3.64×10^{-2}	2.23	2.27×10^{-1}	2.02
-17	—	—	3.61×10^{-2}	2.76
	40 MHz		50 MHz	
Material	K	β	K	β
M3	1.91×10^{-1}	2.45	1.03	2.15
P	2.18×10^{-1}	2.18	6.96×10^{-1}	2.09
67	7.40×10^{-1}	2.04	1.15	2.05
N40	5.18×10^{-1}	2.00	2.08×10^{-1}	2.58
-17	8.25×10^{-2}	2.72	1.86	2.10
	60 MHz		70 MHz	
Material	K	β	K	β
M3	1.76	2.11	—	—
P	1.34	2.04	—	—
67	2.40	1.97	—	—
N40	6.90×10^{-1}	2.25	—	—
-17	1.95	2.16	2.35	2.22

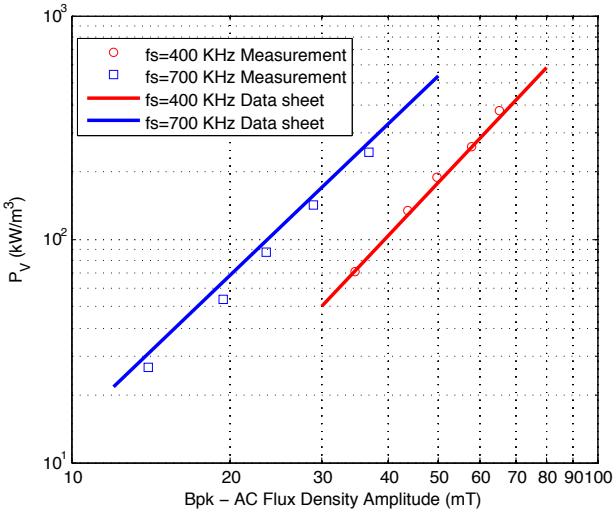

Fig. 9. 3F3 Material Core Loss vs AC Flux Density.

loss prediction is more accurate). This verifies the accuracy and feasibility of our methods.

V. Application Example

To demonstrate application of the measurement techniques, methods and evaluated magnetic materials in rf power conversion, a magnetic-core inductor has been designed and fabricated to replace the original coreless resonant inductor L_S in a VHF (very high frequency) Φ2 inverter [2] [2]. Fig. 10 shows the inverter topology [2]. The switching frequency of the inverter is 30 MHz, and operation is demonstrated with an input voltage of 100 V and an output power of 100 W.

The inductor is designed with a commercial magnetic core T502525T from Ceramic Magnetics, which uses magnetic material N40 in Table I. We select this core for two reasons. Firstly, the magnetic-core inductor fabricated with it has an

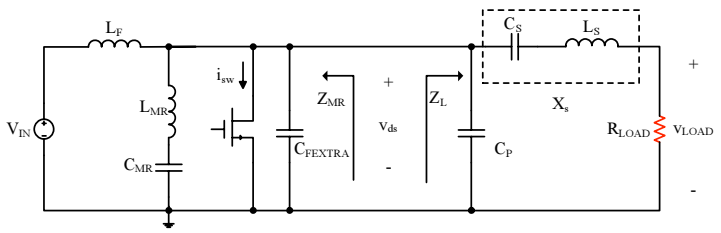

Fig. 10. Class Φ2 inverter. L_S is a resonant inductor.

[2]Both magnetic-core and coreless inductors can be applied in very high frequency power conversion. In some cases, coreless inductors may be better, and in some cases magnetic cores may offer substantial advantage. The detailed methods of selection and comparison among design options are explored in [26].

inductance close to that of the original coreless inductor, which is important to maintain the desired resonant condition of the inverter. Secondly, N40 material has a relatively low loss characteristic and the inductor built with it thus has a high quality factor as desired in this application. This toroidal core has dimensions of OD= 12.7 mm, ID= 6.3 mm, Ht= 6.3 mm and V= 0.60 cm^3. We begin the design by calculating the number of inductor turns:

$$N = \left\lceil \sqrt{\frac{2\pi L}{h\mu_r\mu_0 \ln\left(\frac{d_o}{d_i}\right)}} \right\rceil \tag{16}$$

Notice N should be the nearest integer in (16). Then we get the estimated inductance of the magnetic-core inductor with N turns:

$$L = \frac{N^2 h\mu_r\mu_0}{2\pi} \ln\left(\frac{d_o}{d_i}\right) \tag{17}$$

The original coreless inductor has an inductance of 193 nH. From (16) and (17), we calculate $N = 4$ and $L = 199$ nH. The core loss of the magnetic-core inductor can be estimated by Steinmetz equation. The flux density amplitude in the toroidal core is:

$$B_{pk} = \frac{2\mu_r\mu_0 N I_{L-pk}}{\pi(d_o + d_i)} \tag{18}$$

The inductor current amplitude I_{L-pk} is 2.4 A at the fundamental frequency of 30 MHz, so $B_{pk} = 61$ G. Table II shows the Steinmetz parameters $K = 0.227$ and $\beta = 2.02$ for N40 material at 30 MHZ. The power loss density is thus $P_V = KV_{pk}^{\beta} = 917$ mW/cm^3. The resistance component modeling core loss is:

$$R_{core} = \frac{2P_V V_L}{I_{L-pk}^2} \tag{19}$$

The core is wound with 4 mil thick copper having width $w_{cu} = 0.20$ cm and length $l_{cu} = 8.8$ cm. If the thickness of the foil is much larger than the skin depth (10), the copper resistance can be simply approximated from the foil width, length and skin depth:

$$R_{cu} = \rho \frac{l_{cu}}{w_{cu}\delta} \tag{20}$$

Proximity effects become important for multi-layer winding designs [38]. Our toroidal inductors have only one-layer windings, so the proximity effect is ignored. By (19) and (20), $R_{core} = 0.19\ \Omega$ and $R_{cu} = 0.06\ \Omega$. Though the estimation of R_{cu} may have significant error, the total error of Q_L calculation is still small because $R_{core} \gg R_{cu}$. Calculated from (2), the quality factor is 150, which is high enough to maintain good inverter efficiency.

To verify our design, Fig. 11 shows a curve of measured Q_L vs. current drive level at 30 MHz for a 230 nH inductor wound with 4 turns of foil on the core T502525T. This curve is measured using the technique of Section II. Note that the actual inductor has a measured inductance of 230 nH, which is higher than the originally predicted value of 199 nH. The deviation of the measured inductance from the initially predicted value for the design is due to the variation of material permeability with frequency, the stray inductance owing to flux

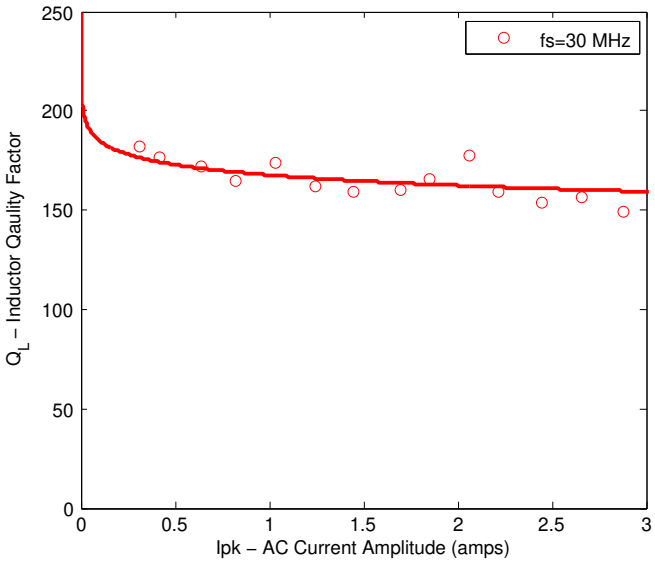

Fig. 11. The Q_L of fabricated inductor withan N40 toroidal core (OD= 12.7 mm, ID= 6.3 mm, Ht= 6.3 mm) with $N = 4$ turns, and $L = 230$ nH.

outside the core, including inductance of the single-turn loop around the center hole of the toroid [28], and stray inductance of the measurement leads. Compared to the inductor built with M3 material in Fig. 2, Q_L in Fig. 11 is very flat for a wide operation range; this can be attributed to the loss parameter β being very close to 2 for N40 material at 30 MHz. At $I_{L-pk} = 2.4$ A, Q_L is about 155 from the curve, which is very close to the value of 150 predicted using (2) and the estimated core loss parameters of Table II. In this design example, the data acquired in Section IV has helped to estimate the loss and quality factor of the magnetic-core inductor accurately.

Fig. 12 shows photographs of the Φ2 inverter prototype before and after the replacement with the magnetic-core inductor. Fig. 13 shows the experimental waveform of the drain to source voltage V_{ds} and the load voltage V_{LOAD} (proportional to inductor current) of the Φ2 inverter with the coreless and the magnetic-core inductors. The Φ2 inverter operates essentially the same with either inductor, maintaining the desired waveform shape and zero voltage switching (ZVS), which is essential for VHF switching. The load voltage V_{LOAD} of the magnetic-core inductor is a little lower because the magnetic-core inductor has a higher inductance than the original coreless inductor [2].

In Table III, the coreless inductor and the magnetic-core inductor are compared in terms of their parameters and performance. Energy density of the inductors is defined as:

$$E_V = \frac{LI_{L-pk}^2}{2V} \tag{21}$$

where V can be the physical volume of the inductor or the storage space of the magnetic field depending on what is of interest. Because most of the flux is kept inside a toroidal core, the storage space of the magnetic field is approximately equal to the physical volume of the inductor in the toroidal magnetic-core design. However, they are unequal for a coreless solenoid inductor. In [47], it is shown that shielding influences

(a) Φ2 inverter with the coreless inductor L_S before the replacement

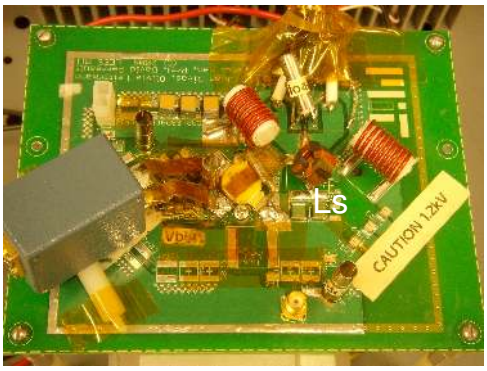

(b) Φ2 inverter with the magnetic-core inductor L_S after the replacement

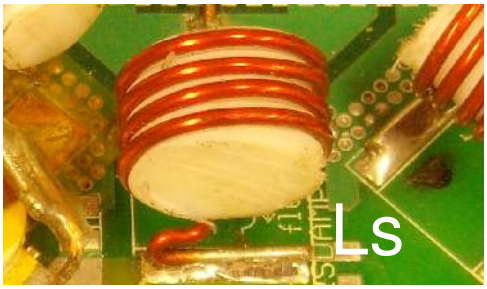

(c) Coreless inductor L_S

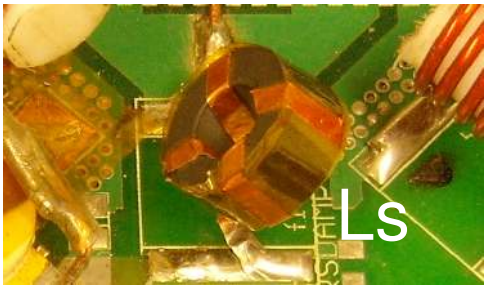

(d) Magnetic-core inductor L_S

Fig. 12. Photographs of the Φ2 inverter prototype before (a, c) and after (b, d) replacement of the coreless inductor with a magnetic-core inductor.

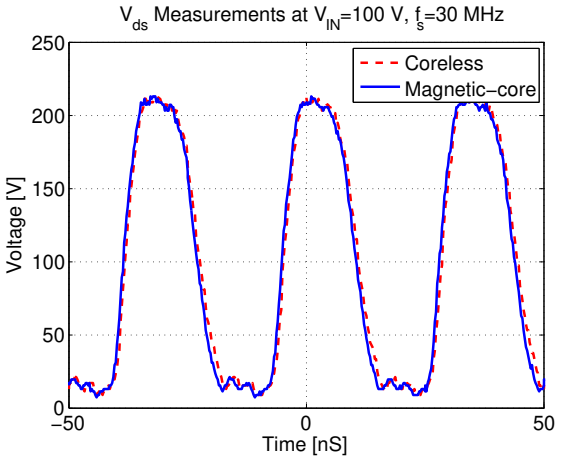

(a) V_{ds}

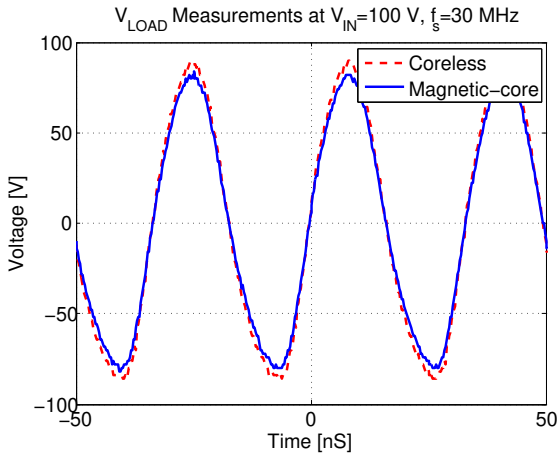

(b) V_{LOAD}

Fig. 13. Drain to source voltage V_{ds} and inverter load voltage V_{LOAD} for the Φ2 inverter with coreless and magnetic-core inductors L_S.

the inductance of a solenoidal coil in free space less than 10% if $\frac{d}{d_s} > 0.5$ and $\frac{(l_s - l)}{2} = 0.25 d_s$. d and l are the outside diameter and length of the solenoid, and d_s and l_s are the outside diameter and length of the shield. From this result, we can think of the field storage of a coreless solenoid as approximately limited in a cylindrical space with $d_s = 2d$ and $l_s = 0.5 d_s + l$. Calculated from d and l in Table III, $d_s = 32.0$ mm, $l_s = 25$ mm and the volume for magnetic field storage is 20166 mm^3 for the coreless solenoid inductor.

In Table III, the toroidal magnetic-core inductor has a somewhat lower quality factor Q_L than the coreless solenoid (150 vs. 190), but has only one third of the physical volume, and lower profile. Even accounting for the proportionate scaling of Q_L with linear dimension for the coreless solenoid [48], [49], the magnetic-core inductor provides a substantial volumetric advantage over that achievable with a coreless design in this application. When considering the field energy storage volume of the two designs, the advantage of the magnetic-core design is even more impressive, yielding a factor of 40 higher energy density. Compared to the coreless solenoid, the toroidal magnetic-core inductor keeps most of flux inside, has much better shielding for electromagnetic fields, and should thus have reduced EMI/EMC. This illustrates the fact that with suitable magnetic materials, magnetic-core designs

TABLE III
COMPARISON BETWEEN THE CORELESS INDUCTOR AND MAGNETIC-CORE INDUCTOR

	Coreless Inductor [2]	Magnetic-core Inductor
Type	Solenoid coreless	Toroidal magnetic core
Design Parameters	4 turns AWG 16 wire on a $5/8$ in. diam. Teflon former with 12 turns/in. threads	4 turns copper foil wound on the core T502525T. The core material is N40 from Ceramic Magnetics in Table I. The foil winding has width $w_{cu} = 0.079$ in and thickness $t_{cu} = 4$ mil.
Measured Inductance	193 nH	230 nH
Measured Q_L	190	150
Dimensions	Diameter $d = 1.60$ cm and length $l = 0.90$ cm	OD= 1.27 cm, ID= 0.63 cm and Ht= 0.63 cm
Physical Volume	1.81 cm^3	0.602 cm^3
Energy Density of Physical Volume	0.302×10^{-6} J/cm^3	1.15×10^{-6} J/cm^3
Field Storage Volume	20.2 cm^3	0.602 cm^3
Energy Density of Field Storage Volume	2.71×10^{-8} J/cm^3	1.15×10^{-6} J/cm^3
Inverter Efficiency	$\approx 93\%$ [2]	

are effective in power applications even at several tens of megahertz.

VI. Conclusion

In this paper, the loss characteristics of several commercial rf magnetic materials are investigated for power conversion applications at very high frequencies (10 MHz to 100 MHz). An experimental method is proposed that provides a direct measurement of inductor quality factor as a function of current at VHF frequencies, and enables indirect calculation of core loss as a function of flux density. The loss characteristics of several rf magnetic materials are further extracted based on the proposed method, and are tabulated and compared as a function of current at VHF frequencies. Possible sources of error using this method are analyzed, and means to address them are presented. A magnetic-core inductor fabricated using one of the evaluated magnetic materials has been applied successfully in an rf resonant power inverter, demonstrating the efficiency of low-permeablity rf materials for power applications in the low VHF range. It is hoped that the presented data and methods will be of value in the design of magnetic components for very high frequency applications.

Acknowledgment

The authors would like to acknowledge the generous support of this work provided by Sheila and Emmanuel Landsman. The authors also acknowledge the support of the Interconnect Focus Center, one of five research centers funded under the Focus Center Research Program, a DARPA and Semiconductor Research Corporation Program.

References

[1] J. Rivas, "Radio frequency dc-dc power conversion," Ph.D. dissertation, Massachusetts Institute of Technology, Sep. 2006.
[2] J. Rivas, Y. Han, O. Leitermann, A. Sagneri, and D. Perreault, "A high-frequency resonant inverter topology with low-voltage stress," *IEEE Trans. Power Electron.*, vol. 23, no. 4, pp. 1759–1771, Jul. 2008.
[3] D. Hamill, "Class DE inverters and rectifiers for dc-dc conversion," *27th IEEE Power Electronics Specialists Conf.*, vol. 1, pp. 854–860, Jun. 1996.
[4] N. Sokal and A. Sokal, "Class E-A new class of high-efficiency tuned single-ended switching power amplifiers," *IEEE J. Solid-State Circuits*, vol. 10, no. 3, pp. 168–176, Jun. 1975.
[5] N. Sokal, "Class-E rf power amplifiers," *QEX*, pp. 9–20, Jan./Feb. 2001.
[6] R. Frey, "High voltage, high efficiency MOSFET rf amplifiers - design procedure and examples," Advanced Power Technology, Application Note APT0001, 2000.
[7] ——, "A push-pull 300-watt amplifier for 81.36 MHz," Advanced Power Technology, Application Note APT9801, 1998.
[8] ——, "500w, class E 27.12 MHz amplifier using a single plastic MOSFET," Advanced Power Technology, Application Note APT9903, 1999.
[9] M. Iwadare and S. Mori, "Even harmonic resonant class E tuned power amplifer without rf choke," *Electron. and Commun. in Japan (Part I: Commun.)*, vol. 79, no. 2, pp. 23–30, Jan. 1996.
[10] S. Kee, I. Aoki, A. Hajimiri, and D. Rutledge, "The class-E/F family of ZVS switching amplifiers," *IEEE Trans. Microw. Theory Tech.*, vol. 51, no. 6, pp. 1677–1690, Jun. 2003.
[11] A. Sagneri, "Design of a very high frequency dc-dc boost converter," Master's thesis, Massachusetts Institute of Technology, Feb. 2007.
[12] W. Bowman, F. Balicki, F. Dickens, R. Honeycutt, W. Nitz, W. Strauss, W. Suiter, and N. Ziesse, "A resonant dc-to-dc converter operating at 22 Megahertz," *3rd Annu. IEEE Applied Power Electronics Conf. and Expo.*, pp. 3–11, Feb. 1988.
[13] R. Pilawa-Podgurski, A. Sagneri, J. Rivas, D. Anderson, and D. Perreault, "Very-high-frequency resonant boost converters," *IEEE Trans. Power Electron.*, vol. 24, no. 6, pp. 1654–1665, Jun. 2009.
[14] R. Gutmann, "Application of RF circuit design principles to distributed power converters," *IEEE Trans. Ind. Electron. Contr. Instrum.*, vol. 27, no. 3, pp. 156–164, Aug. 1980.
[15] J. Jóźwik and M. Kazimierczuk, "Analysis and design of class-e^2 dc/dc converter," *IEEE Trans. Ind. Electron.*, vol. 37, no. 2, pp. 173–183, Apr. 1990.
[16] S. Ajram and G. Salmer, "Ultrahigh frequency dc-to-dc converters using GaAs power switches," *IEEE Trans. Power Electron.*, vol. 16, no. 5, pp. 594–602, Sep. 2001.
[17] R. Steigerwald, "A comparison of half-bridge resonant converter topologies," *IEEE Trans. Power Electron.*, vol. 3, no. 2, pp. 174–182, Apr. 1988.
[18] R. Redl and N. Sokal, "A 14-MHz 100-watt class E resonant converter: principle, design considerations and measured performance," *17th IEEE Power Electronics Specialists Conf.*, pp. 68–77, 1986.
[19] W. Tabisz and F. Lee, "Zero-voltage-switching multi-resonant technique-a novel approach to improve performance of high frequency quasi-resonant converters," *19th IEEE Power Electronics Specialists Conf.*, pp. 9–17, Apr. 1988.
[20] F. Lee, "High-frequency quasi-resonant converter technologies," *Proceedings of the IEEE*, vol. 76, no. 4, pp. 377–390, Apr. 1988.
[21] Y. Han and D. J. Perreault, "Analysis and design of high efficiency matching networks," *IEEE Trans. Power Electron.*, vol. 21, no. 5, pp. 1484–1491, Sep. 2006.
[22] C. Bowick, *RF Circuit Design*. London, UK: Newnes, 1997, ch. 3.
[23] W. Everitt and G. Anner, *Communication Engineering*, 3rd ed. McGraw-Hill Book Company, 1956, ch. 11.
[24] T. Lee, *The Design of CMOS Radio-Frequency Integrated Circuits*, 2nd ed. Cambridge, UK: Cambridge University Press, 2004, ch. 3.
[25] E. Gilbert, "Impedance matching with lossy components," *IEEE Trans. Circuits Syst.*, vol. 22, no. 2, pp. 96–100, Feb. 1975.
[26] Y. Han and D. Perreault, "Inductor design methods with low-permeability rf core materials," *IEEE Energy Conversion Congress and Exposition*, pp. 4376–4383, Sep. 2010.
[27] Y. Han, G. Cheung, A. Li, C. Sullivan, and D. Perreault, "Evaluation of magnetic materials for very high frequency power applications," *39th IEEE Power Electronics Specialists Conf.*, pp. 4270–4276, Jun. 2008.
[28] C. Sullivan, W. Li, S. Prabhakaran, and S. Lu, "Design and fabrication of low-loss toroidal air-core inductors," *38th IEEE Power Electronics Specialists Conf.*, pp. 1757–1759, Jun. 2007.

[29] G. Bertotti, "General properties of power losses in soft ferromagnetic materials," *IEEE Trans. Magn.*, vol. 24, no. 1, pp. 621–630, Jan. 1988.
[30] J. Goodenough, "Summary of losses in magnetic materials," *IEEE Trans. Magn.*, vol. 38, no. 5, pp. 3398–3408, Sep. 2002.
[31] W. Roshen, "A practical, accurate and very general core loss model for nonsinusoidal waveforms," *IEEE Trans. Power Electron.*, vol. 22, no. 1, pp. 30–40, Jan. 2007.
[32] J. Li, T. Abdallah, and C. Sullivan, "Improved calculation of core loss with nonsinusoidal waveforms," *36th Annual Meeting of IEEE Industry Applications Society*, vol. 4, pp. 2203–2210, Sep./Oct. 2001.
[33] K. Venkatachalam, C. Sullivan, T. Abdallah, and H. Tacca, "Accurate prediction of ferrite core loss with nonsinusoidal waveforms using only steinmetz parameters," *2002 IEEE Workshop on Computers in Power Electronics*, pp. 36–41, Jun. 2002.
[34] A. Goldberg, "Development of magnetic components for 1-10 MHz dc/dc converters," Ph.D. dissertation, Massachusetts Institute of Technology, Sep. 1988.
[35] "IEEE standard for test procedures for magnetic cores," IEEE, Standard 393-1991, Mar. 1992.
[36] "Cores made of soft magnetic materials–measuring methods," IEC, International Standard 62044-1, 2002-2005.
[37] M. Mu, Q. Li, D. Gilham, F. Lee, and K. Ngo, "New core loss measurement method for high frequency magnetic materials," *IEEE Energy Conversion Congress and Exposition*, pp. 4384–4389, Sep. 2010.
[38] R. Erickson and D. Maksimović, *Fundamentals of Power Electronics*, 2nd ed. Springer Science and Business Media Inc., 2001, ch. 13.
[39] C. Steinmetz, "On the law of hysteresis," *Proc. of the IEEE*, vol. 72, pp. 197–221, Feb. 1984.
[40] M. Albach, T. Durbaum, and A. Brockmeyer, "Calculating core losses in transformers for arbitrary magnetizing currents a comparison of different approaches," *27th IEEE Power Electronics Specialists Conf.*, vol. 2, pp. 1463–1468, Jun. 1996.
[41] J. Reinert, A. Brockmeyer, and R. D. Doncker, "Calculation of losses in ferro- and ferrimagnetic materials based on the modified steinmetz equation," *IEEE Trans. Ind. Applicat.*, vol. 37, no. 4, pp. 1055–1061, Jul./Aug. 2001.
[42] A. Brockmeyer, "Dimensionierungswekzeug f"ur magnetische bauelemente in stromrichteranwendungen," Ph.D. dissertation, Aachen University of Technology, 1997.
[43] S. Mulder, "Power ferrite loss formulas for transformer design," *Power Conversion and Intelligent Motion*, vol. 21, no. 7, pp. 22–31, Jul. 1995.
[44] E. Snelling, *Soft ferrites, properties and applications*, 2nd ed. Butterworths, 1988.
[45] *Data Sheet: 3F3 Material Specification*, Ferroxcube, Sep. 2004.
[46] *Design of Planar Power Transformers*, Ferroxcube, May 1997.
[47] T. Simpson, "Effect of a conducting shield on the inductance of an air-core solenoid," *IEEE Trans. Magn.*, vol. 35, no. 1, pp. 508–515, Jan. 1999.
[48] D. Perreault, J. Hu, J. Rivas, Y. Han, O. Leitermann, R. Pilawa-Podgurski, A. Sagneri, and C. Sullivan, "Opportunities and challenges in very high frequency power conversion," *24th Annu. IEEE Applied Power Electronics Conf. and Expo.*, pp. 1–14, Feb. 2009.
[49] T. Lee, *Planar Microwave Engineering: A Practical Guide to Theory, Measurement, and Circuits*. Cambridge University Press, 2004, ch. 6.